Feedback-based safe gradient flow for optimal regulation of virtual power plants

Antonin Colot[1] , Bertrand Cornélusse[1], Jorge Cortés[2], Emiliano Dall'Anese[3]*

[1]*Department of Electrical Engineering and Computer Science, University of Liège, Belgium*
[2]*Department of Mechanical and Aerospace Engineering, University of California San Diego, USA*
[3]*Department of Electrical and Computer Engineering, Boston University, USA*
**E-mail: antonin.colot@uliege.be*

Keywords: DISTRIBUTED ENERGY RESOURCES, OPTIMAL POWER FLOW, VIRTUAL POWER PLANTS, UNBALANCED THREE-PHASE NETWORK

Abstract

This paper considers the problem of controlling distributed energy resources (DERs) in a distribution network (DN); the paper focuses on the voltage regulation task and on the concept of *virtual power plant* (VPP). For the latter, we envision an aggregation of DERs as a VPP that tracks power setpoints at the point of common coupling to provide ancillary services to the bulk power system. We propose a feedback-based controller that pursues solutions to a time-varying AC optimal power flow problem. This controller ensures voltage constraints are met in real time, assuming no voltage measurement errors. The feedback from the system mitigates the controller sensitivity to model uncertainties and eliminates the need for measurements of uncontrollable loads at every node. The feedback-based controller is tested on the IEEE37-node system with delta and wye-connected devices in a strongly unbalanced configuration.

1 Introduction

Rising energy costs and government incentives for promoting the adoption of renewable energy sources (RESs) create a significant change in distribution networks (DN). Increasing integration of RESs creates bidirectional power flows that can jeopardize power quality, operational efficiency, and reliability [1]. Traditionally, slow-acting controllers, such as load tap changers or switched capacitors, regulate voltages in DNs, but the variability of RES production renders slow-acting controllers inefficient and can shorten their lifespan [2]. At the transmission level, large-scale synchronous generators provide voltage and frequency regulation, but the decommissioning of conventional power plants challenges power system stability. On the other hand, the continuous improvements in power electronic converters pave the way for new regulation techniques. Distributed energy resources (DERs) can now provide ancillary services to the bulk power system while mitigating voltage issues within DNs [3].

A *virtual power plant* (VPP) [4] is an aggregation of DERs in a DN that provides ancillary services to the bulk power system while satisfying operational constraints within the DN. A traditional VPP regulation approach involves solving an AC optimal power flow (AC-OPF) problem in an open-loop fashion to dispatch DER setpoints. Such an approach is inadequate for real-time optimization for three reasons [5]. First, it requires measuring the net power injections at every node, which might be hard to achieve in DNs. Second, the DN dynamics might be faster than the time required to solve the AC-OPF because of the computational complexity, thus leading to outdated setpoints. Finally, the AC-OPF is solved in an open-loop fashion and is therefore prone to modeling errors. One can opt for distributed approaches to reduce the AC-OPF problem complexity, but these methods may be slow to converge, and the obtained setpoints may eventually be outdated [6].

Other approaches suggest using learning-based methods. One advantage is the speed-up during the inference phase when the model predicts a solution to the AC-OPF problem [7, 8]. On the other hand, those methods suffer from two significant drawbacks [9]: data availability and the lack of a worst-case guarantee. In some critical applications, learning-based AC-OPF solvers cannot always satisfy operational constraints. To address those challenges, [9] proposes a physics-informed neural network that alleviates data quality and size requirements and provides guarantees for constraints violation. However, these methods require knowledge of the net power injections at every node.

In recent years, several works have focused on online or real-time algorithms for solving the AC-OPF problem [6]. The task is to design a real-time feedback controller that pursues an optimal trajectory for the AC-OPF problem while guaranteeing closed-loop system stability. In particular, our recent work [10] leverages the theory of control barrier functions to ensure that the feedback-based optimization method always satisfies voltage constraints. The safe gradient flow has first been proposed in [11], but the novelty in [10] is the introduction of the feedback to track varying grid conditions. This method pursues time-varying solutions to an AC-OPF problem.

Contributions: In this paper, we leverage the algorithm developed in [10] and extend it to a 3-phase unbalanced DN, with wye and delta-connected sources. We consider the problem of regulating a VPP such that it can track power references at the substation while meeting voltage constraints within the

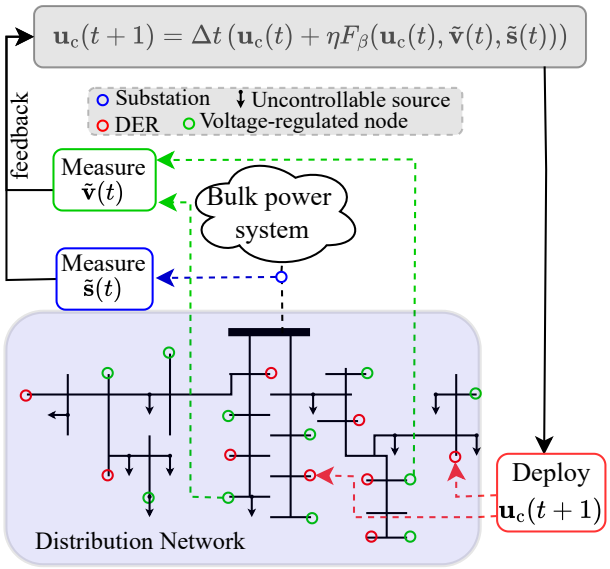

Fig. 1: Feedback-based safe gradient flow controller

DN. Figure 1 illustrates the working principle of the algorithm.

The power system model and the AC-OPF are introduced in Section 2, in Section 3 the feedback-based safe gradient flow controller is presented, we show numerical results in Section 4, and finally, Section 5 concludes the paper.

2 Problem formulation

2.1 Power system model

We consider a generic three-phase DN with $N+1$ nodes* and a combination of wye-connected and delta-connected sources. The node 0 is taken to be the substation node, while $\mathcal{N} := \{1, ..., N\}$ is the set of remaining nodes. Let $\mathbf{s}_j^Y := \{s_j^a, s_j^b, s_j^c\}^\top$ denote the vector of net complex phase-to-ground power injections on each phase $\{a, b, c\}$ at node j. Similarly, let $\mathbf{s}_j^\Delta := \{s_j^{ab}, s_j^{bc}, s_j^{ca}\}^\top$ denote the vector of net complex phase-to-phase power injections at node j on each phase connections $\{ab, bc, ca\}$. Let us denote $\mathbf{v}_j := (v_j^a, v_j^b, v_j^c)^\top, \mathbf{i}_j := (i_j^a, i_j^b, i_j^c)^\top, \mathbf{i}_j^\Delta := (i_j^{ab}, i_j^{bc}, i_j^{ca})^\top$ the vectors collecting the phase-to-ground voltages, the phase current injections, and the phase-to-phase currents for node j, respectively. We define the following quantities $\mathbf{v} := \{(\mathbf{v}_j)^\top\}_{j\in\mathcal{N}}^\top, \mathbf{i} := \{(\mathbf{i}_j)^\top\}_{j\in\mathcal{N}}^\top, \mathbf{i}^\Delta := \{(\mathbf{i}_j^\Delta)^\top\}_{j\in\mathcal{N}}^\top, \mathbf{s}^Y := \{(\mathbf{s}_j^Y)^\top\}_{j\in\mathcal{N}}^\top, \mathbf{s}^\Delta := \{(\mathbf{s}_j^\Delta)^\top\}_{j\in\mathcal{N}}^\top$ to express the power flow equations in matrix form [12]:

$$\begin{aligned} \operatorname{diag}\left(H^\top(\mathbf{i}^\Delta)^*\right)\mathbf{v} + \mathbf{s}^Y &= \operatorname{diag}(\mathbf{v})\mathbf{i}^*, \\ \mathbf{s}^\Delta &= \operatorname{diag}(H\mathbf{v})(\mathbf{i}^\Delta)^*, \\ \mathbf{i} &= Y_{L0}\mathbf{v}_0 + Y_{LL}\mathbf{v}, \\ \mathbf{s}_0^Y &= \operatorname{diag}(\mathbf{v}_0)(Y_{00}^*\mathbf{v}_0^* + Y_{0L}^*\mathbf{v}^*), \end{aligned} \tag{1}$$

where $Y_{00}, Y_{L0}, Y_{0L}, Y_{LL}$ denote the submatrices of the three-phase bus admittance matrix

$$Y := \begin{bmatrix} Y_{00} & Y_{0L} \\ Y_{L0} & Y_{LL} \end{bmatrix} \in \mathbb{C}^{3(N+1)\times 3(N+1)}, \tag{2}$$

that can be derived from the network topology and the π-model of the distribution lines, and H is a block-diagonal matrix defined by

$$H := \operatorname{diag}(\Gamma),\ \Gamma := \begin{bmatrix} 1 & -1 & 0 \\ 0 & 1 & -1 \\ -1 & 0 & 1 \end{bmatrix}. \tag{3}$$

One can find the solution $\mathbf{v}$ of the set of equations (1), with known $\mathbf{s}^Y, \mathbf{s}^\Delta$ and $\mathbf{v}_0$, using the following fixed-point equation [12]:

$$\mathbf{v} = \mathbf{w} + Y_{LL}^{-1}\left(\operatorname{diag}(\mathbf{v}^*)^{-1}(\mathbf{s}^Y)^* + H^\top \operatorname{diag}(H\mathbf{v}^*)^{-1}(\mathbf{s}^\Delta)^*\right), \tag{4}$$

where $\mathbf{w} := -Y_{LL}^{-1}Y_{L0}\mathbf{v}_0$ is the zero-load voltage.

For convenience, we define the algebraic maps $V := \mathbb{C}^{3N+3N+3} \mapsto \mathbb{C}^{3N}$ and $S := \mathbb{C}^{3N+3N+3} \mapsto \mathbb{C}^3$ such that $\mathbf{v} = V(\mathbf{s}^Y, \mathbf{s}^\Delta, \mathbf{v}_0)$ and $\mathbf{s}_0 = \mathbf{s}_0^Y = S(\mathbf{s}^Y, \mathbf{s}^\Delta, \mathbf{v}_0)$. These maps correspond to the *practical* solution –high voltage, low line currents solution– of the power flow equations described in (1).

Remark 1. *The existence of the maps V and S are based on the Implicit Function Theorem, and the results of, e.g., [13]. Notice that one can only obtain an analytical formulation of such maps in particular conditions. Also, replacing $\mathbf{v}$ by $\mathbf{w}$ on the right-hand side of the fixed-point equation* (4) *gives a first-order approximation of the map V for $\mathbf{s}^Y \approx \mathbf{0}, \mathbf{s}^\Delta \approx \mathbf{0}$.*

2.2 Problem setup

The goal is to coordinate DERs injections to regulate voltage magnitudes within the DN while tracking power reference setpoints at the substation $S_{\text{set}} := \{P_{\phi,\text{set}}, Q_{\phi,\text{set}}\}_{\phi\in\{a,b,c\}}^\top$, where $P_{\phi,\text{set}}, Q_{\phi,\text{set}}$ represent the active and reactive power setpoint at the substation for each phase ϕ, respectively. We formulate the following optimization problem:

$$\begin{aligned} \min_{\mathbf{s}^Y, \mathbf{s}^\Delta, \mathbf{v}_0} \quad & f(\mathbf{s}^Y, \mathbf{s}^\Delta, \mathbf{v}_0) \\ \text{s.t.} \quad & \mathbf{v}_{\min} \le |V(\mathbf{s}^Y, \mathbf{s}^\Delta, \mathbf{v}_0)| \le \mathbf{v}_{\max}, \\ & -E \le S(\mathbf{s}^Y, \mathbf{s}^\Delta, \mathbf{v}_0) - S_{\text{set}} \le E, \\ & \mathbf{s}^Y, \mathbf{s}^\Delta \in \mathcal{S}, \end{aligned} \tag{5}$$

where $\mathbf{v}_{\max}, \mathbf{v}_{\min}$ denote the vectors of maximum and minimum voltage magnitudes, E is a scalar that can be arbitrary

Notation: upper-case (lower-case boldface) letters are used for matrices (column vectors); $(.)^\top$ denotes transposition and $(.)^*$ the complex-conjugate; j the imaginary unit and $|.|$ the absolute value of a number. If we consider a given vector $\mathbf{x} \in \mathbb{R}^N$, $\operatorname{diag}()$ returns a $N \times N$ matrix with the element of $\mathbf{x}$ in its diagonal. For vectors $\mathbf{x} \in \mathbb{R}^N$ and $\mathbf{u} \in \mathbb{R}^M$, $\|\mathbf{x}\|_2$ denotes the ℓ_2-norm and $(\mathbf{x}, \mathbf{u}) \in \mathbb{R}^{N+M}$ denotes their vector concatenation. $\mathbb{C}$ denotes the set of complex numbers and for a vector $\mathbf{y} \in \mathbb{C}^N$, $\mathcal{R}(\mathbf{y}) \in \mathbb{R}^N$ denotes its real part and $\mathcal{I}(\mathbf{y}) \in \mathbb{R}^N$ its imaginary part.

small to track power reference setpoints and $\mathcal{S}$ represents the hardware limits of DERs, i.e., maximum and minimum power injections. One can design the objective function $f(.)$ to minimize the usage of reactive power compensation or active power curtailment or may favor the minimization of system losses or voltage deviations from a nominal voltage profile. First, for clarity, let us consider the case when the power injection at each node is controllable in problem (5). We will further distinguish controllable and non-controllable sources in the final problem formulation. Also, one can consider other constraints, such as maximum line ampacity. Solving problem (5) is challenging because it contains non-linear constraints and is known to be non-convex. Furthermore, the solution to problem (5) heavily depends on the model parameters (e.g., the elements of Y), and there is no guarantee one can satisfy operational constraints under model uncertainties. In the following section, we propose a feedback-based safe gradient flow controller, built as a quadratic programming problem, incorporating feedback from the system to cope with model uncertainties.

3 Feedback-based safe gradient flow

3.1 Safe Gradient Flow design principle

Consider the admissible set $\mathcal{F} = \{\mathbf{x} \in \mathbb{C}^{3N+3N+3} \mid g(\mathbf{x}) \leq 0\}$, where $\mathbf{x} := (\mathbf{s}^Y, \mathbf{s}^\Delta, \mathbf{v}_0)$ and $g(\mathbf{x})$ is a vector-valued function representing the constraints of problem (5). We can write the problem (5) as:

$$\min_{\mathbf{x}\in\mathcal{F}} f(\mathbf{x}). \tag{6}$$

If $\bar{\mathbf{x}} \in \mathcal{F}$ is a local optimizer of problem (6) and assuming some mild regularity assumptions hold at $\bar{\mathbf{x}}$ (see [10]), then it exists $\bar{\mathbf{y}}$ such that the *Karush-Kuhn-Tucker* (KKT) conditions hold:

$$\nabla f(\bar{\mathbf{x}}) + \frac{\partial g(\bar{\mathbf{x}})}{\partial \mathbf{x}}^\top \bar{\mathbf{y}} = 0, \tag{7a}$$

$$g(\bar{\mathbf{x}}) \leq 0, \bar{\mathbf{y}} \geq 0, (\bar{\mathbf{y}})^\top g(\bar{\mathbf{x}}) = 0. \tag{7b}$$

As proposed in [11], for solving problem (6), one can consider the following control-affine system:

$$\dot{\mathbf{x}} = -\nabla f(\mathbf{x}) - \frac{\partial g(\mathbf{x})}{\partial \mathbf{x}}^\top \mathbf{y}, \tag{8}$$

that can be interpreted as the standard gradient flow, with a *drift term* depending on the control actions $\mathbf{y}$. The general idea is to find the control actions $\mathbf{y}$ such that the admissible set $\mathcal{F}$ is *forward-invariant*; if the system states $\mathbf{x}$ start inside the set $\mathcal{F}$, the state trajectories are confined in that set at all times. Furthermore, if the system states start outside the admissible set $\mathcal{F}$, the system trajectories should converge to the admissible set $\mathcal{F}$. One can obtain the control actions $\mathbf{y}^\sharp$ by solving:

$$\mathbf{y}^\sharp = \arg\min_{\mathbf{y}\in K_\beta(\mathbf{x})} \left\| \frac{\partial g(\mathbf{x})}{\partial \mathbf{x}}^\top \mathbf{y} \right\|_2^2 \tag{9}$$

where the *drift term* is minimized, and the admissible set for $\mathbf{y}$:

$$K_\beta(\mathbf{x}) := \left\{ \mathbf{y} \in \mathbb{C}^{6N+3} \,\middle|\, -\frac{\partial g}{\partial \mathbf{x}} \frac{\partial g}{\partial \mathbf{x}}^\top \mathbf{y} \leq \frac{\partial g}{\partial \mathbf{x}} \nabla f(\mathbf{x}) - \beta g(\mathbf{x}) \right\} \tag{10}$$

is defined such that the set $\mathcal{F}$ is *forward-invariant*, with $\beta > 0$ a design parameter. The set $K_\beta(\mathbf{x})$ is inspired by Control Barrier Functions arguments [14], and obtained considering $\mathcal{F}$ as the safe set, and g as a vector-control barrier function (see [11] for further details). In [11], it is shown that (8) with the control actions obtained solving (9) is equivalent to dynamics of the form $\dot{\mathbf{x}} = F_\beta(\mathbf{x})$ with

$$\begin{aligned} F_\beta(\mathbf{x}) := \arg \min_{\theta\in\mathbb{C}^{3N+3N+3}} \quad & \frac{1}{2} \|\theta + \nabla f(\mathbf{x})\|_2^2 \\ \text{s.t.} \quad & \frac{\partial g(\mathbf{x})}{\partial \mathbf{x}}^\top \theta \leq -\beta g(\mathbf{x}). \end{aligned} \tag{11}$$

3.2 Linear approximation of the three-phase power flow equations

As shown in (11), one needs explicit formulation of the maps $V(.)$ and $S(.)$. As mentioned in Remark 1, there is no explicit formulation for $V(.)$ and $S(.)$. Therefore, we leverage the linear approximations proposed in [12]:

$$\begin{aligned} |V(\mathbf{s}^Y, \mathbf{s}^\Delta, \mathbf{v}_0)| &\approx K^Y \mathbf{x}^Y + K^\Delta \mathbf{x}^\Delta + \mathbf{b}, \\ S(\mathbf{s}^Y, \mathbf{s}^\Delta, \mathbf{v}_0) &\approx G^Y \mathbf{x}^Y + G^\Delta \mathbf{x}^\Delta + \mathbf{c}, \end{aligned} \tag{12}$$

where $\mathbf{x}^Y := ((\mathbf{p}^Y)^\top, (\mathbf{q}^Y)^\top)^\top$ and $\mathbf{x}^\Delta := ((\mathbf{p}^\Delta)^\top, (\mathbf{q}^\Delta)^\top)^\top$ with $\mathbf{p}^Y := \mathcal{R}\{\mathbf{s}^Y\}$, $\mathbf{q}^Y := \mathcal{I}\{\mathbf{s}^Y\}$, $\mathbf{p}^\Delta := \mathcal{R}\{\mathbf{s}^\Delta\}$, $\mathbf{q}^\Delta := \mathcal{I}\{\mathbf{s}^\Delta\}$ collecting the active and reactive power injections. In the following, we detail how to construct the different matrices presented in (12) (see [12] for detailed derivations). We define $(\hat{\mathbf{v}}, \hat{\mathbf{s}}^Y, \hat{\mathbf{s}}^\Delta)$ as a given solution of the fixed-point equation (4). We then write:

$$\begin{aligned} M^Y &:= (Y_{LL}^{-1}\text{diag}(\hat{\mathbf{v}}^*)^{-1}, -jY_{LL}^{-1}\text{diag}(\hat{\mathbf{v}}^*)^{-1}), \\ M^\Delta &:= \left(Y_{LL}^{-1}H^\top \text{diag}(H\hat{\mathbf{v}}^*)^{-1}, -jY_{LL}^{-1}H^\top \text{diag}(H\hat{\mathbf{v}}^*)^{-1}\right), \\ K^Y &:= |\text{diag}(\mathbf{w})|\mathcal{R}\{\text{diag}(\mathbf{w})^{-1}M^Y\}, \mathbf{b} := |\mathbf{w}|, \\ K^\Delta &:= |\text{diag}(\mathbf{w})|\mathcal{R}\{\text{diag}(\mathbf{w})^{-1}M^\Delta\}, \\ G^Y &:= \text{diag}(\mathbf{v}_0)Y_{0L}^*(M^Y)^*, G^\Delta := \text{diag}(\mathbf{v}_0)Y_{0L}^*(M^\Delta)^*, \\ \mathbf{c} &:= \text{diag}(\mathbf{v}_0)\left(Y_{00}^*\mathbf{v}_0^* + Y_{0L}^*\mathbf{w}^*\right). \end{aligned} \tag{13}$$

For the rest of the paper, we consider constant matrices obtained from $(\mathbf{w}, \mathbf{0}, \mathbf{0})$, that is a solution of (1). However, one can improve the quality of the linear approximation by constructing the matrices based on the current operating conditions $(\hat{\mathbf{v}}, \hat{\mathbf{s}}^Y, \hat{\mathbf{s}}^\Delta)$, which requires measuring the voltages and power injections at every node in real-time.

3.3 Design of the controller

First, let us define the vector $\mathbf{u}_\text{c} = ((\mathbf{x}_\text{c}^Y)^\top, (\mathbf{x}_\text{c}^\Delta)^\top) \in \mathbb{C}^U$, where $\mathbf{x}_\text{c}^Y, \mathbf{x}_\text{c}^\Delta$ contain the power injections of the DERs. The number U depends on the number of DERs, and their connection type (1-phase or 3-phase connection). Similarly, we define $\mathbf{u}_\text{nc} = ((\mathbf{x}_\text{nc}^Y)^\top, (\mathbf{x}_\text{nc}^\Delta)^\top) \in \mathbb{C}^{3N+3N-U}$ the vector of non-controllable sources. For simplicity, let us consider that the voltage at the substation $\mathbf{v}_0$ cannot be controlled and is held constant to 1 pu. Furthermore, we consider that, for each controllable source, the feasible set

describing the hardware limits is defined as $\mathcal{S} := \mathcal{S}^Y \cup \mathcal{S}^\Delta$, with $\mathcal{S}^Y := \{0 \leq \mathbf{p}^Y_{j,\phi} \leq \mathbf{p}^Y_{j,\phi,\max}, (\mathbf{p}^Y_{j,\phi})^2 + (\mathbf{q}^Y_{j,\phi})^2 \leq (\mathbf{s}^Y_{j,\phi,\text{nom}})^2, |\mathbf{q}^Y_{j,\phi}| \leq 0.44\mathbf{s}^Y_{j,\phi,\text{nom}}\}_{j\in\mathcal{G}^Y,\phi\in\{a,b,c\}}$, $\mathcal{S}^\Delta := \{0 \leq \mathbf{p}^\Delta_{j,\phi} \leq \mathbf{p}^\Delta_{j,\phi,\max}, (\mathbf{p}^\Delta_{j,\phi})^2 + (\mathbf{q}^\Delta_{j,\phi})^2 \leq (\mathbf{s}^\Delta_{j,\phi,\text{nom}})^2, |\mathbf{q}^\Delta_{j,\phi}| \leq 0.44\mathbf{s}^\Delta_{j,\phi,\text{nom}}\}_{j\in\mathcal{G}^\Delta,\phi\in\{ab,bc,ca\}}$, where $\mathcal{G}^Y$,$\mathcal{G}^\Delta$ are the set of nodes to which wye-connected, delta-connected DERs are connected, respectively. The feasible set $\mathcal{S}$ is such that each phase is constrained independently. Finally, let us denote the vector-valued function $\ell(\mathbf{u}_\text{c})$ such that we can write $\mathcal{S} := \{\mathbf{u}_\text{c} \in \mathbb{C}^U \mid \ell(\mathbf{u}_\text{c}) \leq 0\}$ for simplicity. We now formulate an algorithmic solution to the problem (5):

$$
\begin{aligned}
&F_\beta(\mathbf{u}_\text{c}, \mathbf{u}_\text{nc}) \quad := \\
&\arg\min_{\theta\in\mathbb{C}^U} \quad \frac{1}{2}\left\|\theta + \nabla f(\mathbf{u}_\text{c})\right\|_2^2 \\
&\text{s.t.} \quad K_\text{c}^\top\theta \leq -\beta\left(K_\text{c}^\top\mathbf{u}_\text{c} + K_\text{nc}^\top\mathbf{u}_\text{nc} + \mathbf{b} - \mathbf{v}_\text{max}\right) \\
&\qquad -K_\text{c}^\top\theta \leq -\beta\left(\mathbf{v}_\text{min} - K_\text{c}^\top\mathbf{u}_\text{c} - K_\text{nc}^\top\mathbf{u}_\text{nc} - \mathbf{b}\right) \\
&\qquad G_\text{c}^\top\theta \leq -\beta\left(G_\text{c}^\top\mathbf{u}_\text{c} + G_\text{nc}^\top\mathbf{u}_\text{nc} + \mathbf{c} - S_\text{set} - E\right) \\
&\qquad -G_\text{c}^\top\theta \leq -\beta\left(E - G_\text{c}^\top\mathbf{u}_\text{c} - G_\text{nc}^\top\mathbf{u}_\text{nc} - \mathbf{c} + S_\text{set}\right) \\
&\qquad \nabla\ell(\mathbf{u}_\text{c})^\top\theta \leq -\beta\ell(\mathbf{u}_\text{c}),
\end{aligned}
\tag{14}
$$

where $K_\text{c}, K_\text{nc}, G_\text{c}, G_\text{nc}$ contain the appropriate elements of matrices $K^Y, K^\Delta, G^Y, G^\Delta$. The problem defined in (14) requires the measurements of the non-controllable powers $\mathbf{u}_\text{nc}$ and relies on the power system model (12). Using appropriate measurements, one can construct an optimization-based feedback controller that naturally tracks the time-varying grid conditions. Let us define $\tilde{\mathbf{v}}$ the vector collecting the voltage measurements at each node, and $\tilde{\mathbf{s}}$ the vector collecting the three-phase apparent power at the substation, one can write an approximation of (14) where measurements are appropriately added to the algorithmic solution:

$$
\begin{aligned}
&F_\beta(\mathbf{u}_\text{c}, \tilde{\mathbf{v}}, \tilde{\mathbf{s}}) := \\
&\arg\min_{\theta\in\mathbb{C}^U} \quad \frac{1}{2}\left\|\theta + \nabla f(\mathbf{u}_\text{c})\right\|_2^2 \\
&\text{s.t.} \quad \beta\left(\mathbf{v}_\text{min} - \tilde{\mathbf{v}}\right) \leq K_\text{c}^\top\theta \leq -\beta\left(\tilde{\mathbf{v}} - \mathbf{v}_\text{max}\right) \\
&\qquad \beta\left(E - \tilde{\mathbf{s}} + S_\text{set}\right) \leq G_\text{c}^\top\theta \leq -\beta\left(\tilde{\mathbf{s}} - S_\text{set} - E\right) \\
&\qquad \nabla\ell(\mathbf{u}_\text{c})^\top\theta \leq -\beta\ell(\mathbf{u}_\text{c}).
\end{aligned}
\tag{15}
$$

Remark 2. *The number of constraints in problem* (15) *depends on the number of DERs and the number of voltage-regulated nodes. If the system operator enforces voltage limits on a subset of the set of nodes: $\mathcal{M} \subset \mathcal{N}$, one needs only voltage measurements at nodes that belong to that subset $\mathcal{M}$. That is a major difference compared to traditional techniques to solve AC-OPF which require load measurements at every node (as shown in problem* (14) *for instance).*

We implement the following controller:

$$
\mathbf{u}_\text{c}(t+1) = \Delta t\left(\mathbf{u}_\text{c}(t) + \eta F_\beta(\mathbf{u}_\text{c}(t), \tilde{\mathbf{v}}(t), \tilde{\mathbf{s}}(t))\right), \tag{16}
$$

which is the forward Euler discretization of the feedback controller $\dot{\mathbf{u}}_\text{c} = \eta F_\beta(\mathbf{u}_\text{c}, \tilde{\mathbf{v}}, \tilde{\mathbf{s}})$, with η as controller gain.

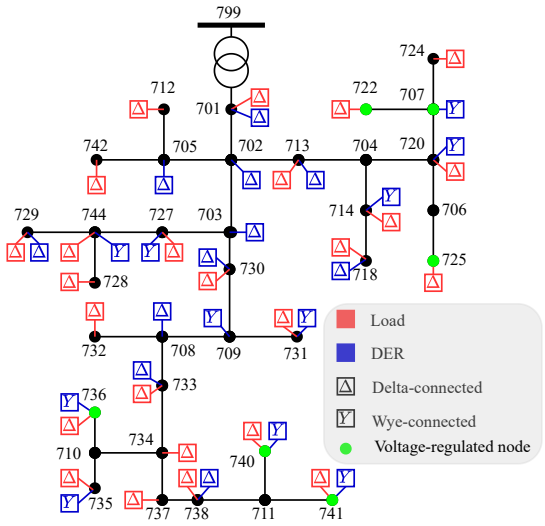

Fig. 2: Modified IEEE37-node feeder

Remark 3. *Notice that* $\mathbf{u}_\text{c}$ *in* (15) *can be obtained from measurements of the DERs' injected powers, rather than coming from the previous setpoints deployed. This is needed if the DERs' controllers are not guaranteed to implement the power setpoints, i.e., if there is a deviation between* $\mathbf{u}_\text{c}$ *and what is deployed.*

4 Experimental results

4.1 Simulation setup

We consider the IEEE37-node feeder shown in Fig. 2 with a 4.8 kV operating voltage. We modified the original benchmark, which contained only delta-connected loads, to incorporate delta and wye-connected DERs. We did not implement DERs' dynamics as they are considered much faster than the controller dynamics. The power setpoints are instantaneously implemented. We only consider PV plants as DERs, with the hardware limits defined by the set $\mathcal{S}$ and $\mathbf{p}_\text{max}$ representing the available power derived from the solar irradiance. We also define the following cost function:

$$
\begin{aligned}
&\sum_{j\in\mathcal{G}^Y}\sum_{\phi\in\{a,b,c\}} c_p(\mathbf{p}^Y_{j,\phi} - \mathbf{p}^Y_{j,\phi,\max})^2 + c_q(\mathbf{q}^Y_{j,\phi})^2 \\
&+ \sum_{j\in\mathcal{G}^\Delta}\sum_{\phi\in\{ab,bc,ca\}} c_p(\mathbf{p}^\Delta_{j,\phi} - \mathbf{p}^\Delta_{j,\phi,\max})^2 + c_q(\mathbf{q}^\Delta_{j,\phi})^2,
\end{aligned}
\tag{17}
$$

such that the active power curtailment and the usage of reactive power are penalized, with $c_p = 3$ and $c_q = 1$. The load profiles and maximum available power aggregated for each phase with a granularity of 10 seconds are shown in Fig. 3. The network is strongly unbalanced.

The results obtained with the feedback-based safe gradient flow (SGF) are compared with the results of the problem (5) with the linear model of the 3-phase power flow equations (12). The latter corresponds to a linear formulation of the AC-OPF (L-AC-OPF) solved in an open-loop fashion. We consider that

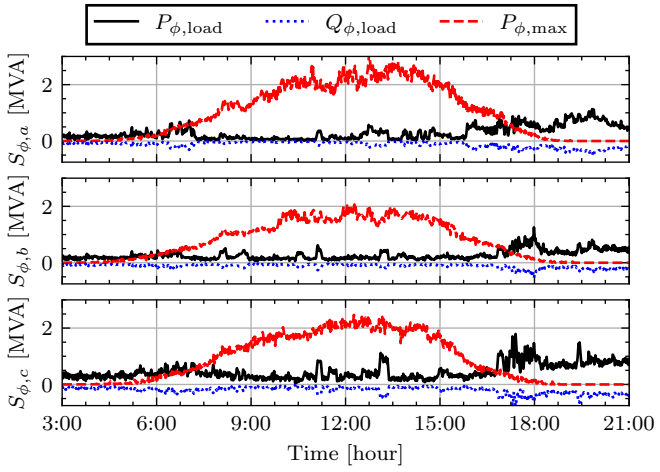

Fig. 3: Aggregated load profiles and maximum power available for DERs per phase

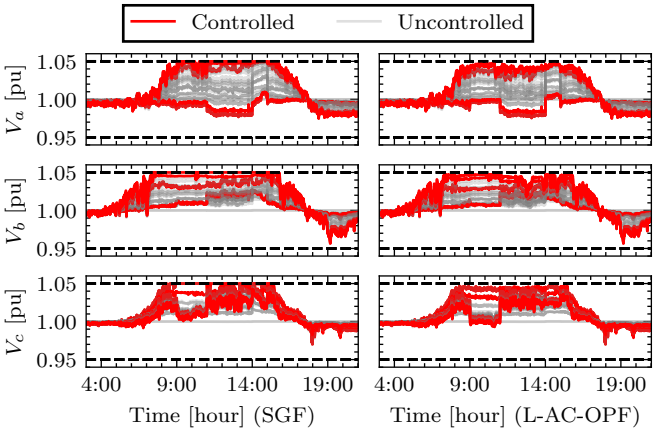

Fig. 4: Voltage magnitudes with SGF and L-AC-OPF algorithms

the SGF receives new measurements, computes new power setpoints and DERs deploy the new power setpoints every second, while the grid conditions ($\mathbf{u}_{\text{nc}}$) change every 10 seconds. We enforce voltage limits, $\mathbf{v}_{\min} = 0.95, \mathbf{v}_{\max} = 1.05$, only on a subset of nodes, highlighted in green in Fig. 2. These nodes have been selected such that the voltage magnitudes of the other nodes stay within the lower and upper voltage limits. We also enforce power tracking at the substation from hours $9:00$ to $11:00$ and from hours $14:00$ to $15:00$. Finally, we consider two scenarios, one with accurate estimation of line impedances, and the other with the line impedances underestimated by 20%. It influences the admittance matrix, and therefore the linear model parameters.

Results with no error in the admittance matrix: In Fig. 4, we compare the voltage magnitudes for different phases when the power setpoints are obtained from the L-AC-OPF and SGF algorithms. One can see that the voltage magnitudes of voltage-regulated nodes stay within the limits. However, while the voltage constraints are tight for SGF, the L-AC-OPF yields lower voltage magnitudes. This is due to the linear model, which overestimates the voltage magnitudes for the L-AC-OPF algorithm, while the SGF algorithm uses voltage measurements. Fig. 5 shows that both algorithms can track the power setpoints at the substation from hours $9:00$ to $11:00$ and from hours $14:00$ to $15:00$. However, the error for the L-AC-OPF is larger than the error for the SGF because of the linear model inaccuracy. We show both algorithms' DERs active power injections in Fig. 6. There is more active power curtailment with L-AC-OPF than with SGF because the linear model overestimates the voltage magnitudes, forcing the L-AC-OPF to produce a greater effort. This is also reflected in the value of the cost function as the total cumulative cost over the day is 44.030 for the SGF and 65.201 for L-AC-OPF.

Results with error in the admittance matrix: In Fig. 7, we compare the voltage magnitudes for the two algorithms when

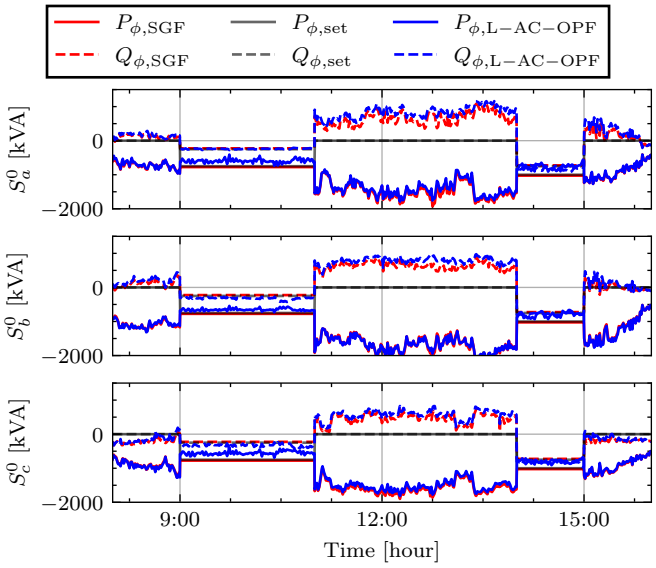

Fig. 5: Power tracking at the substation with SGF and L-AC-OPF algorithms

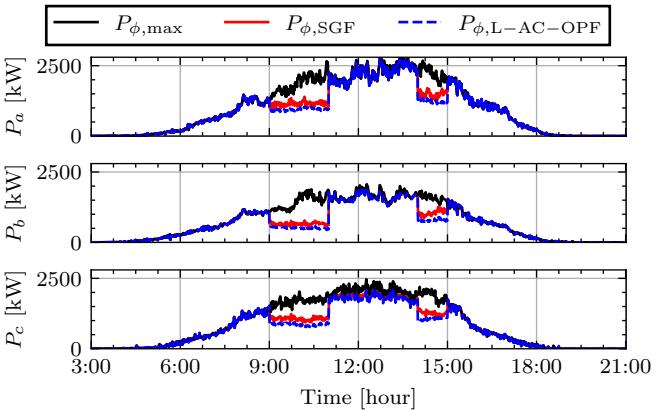

Fig. 6: Available active power and DERs active power injections with SGF and L-AC-OPF algorithms

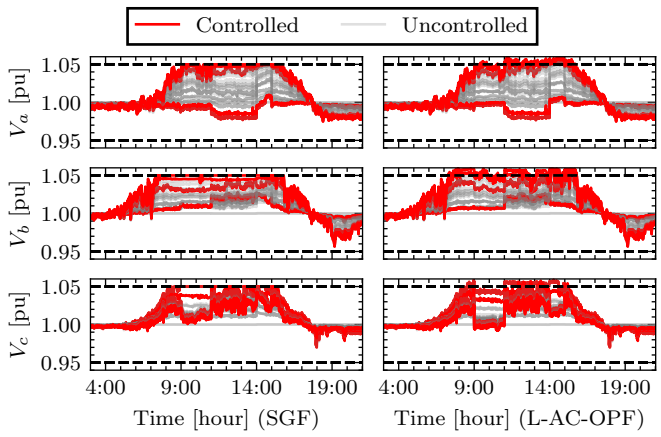

Fig. 7: Voltage magnitudes with SGF and L-AC-OPF algorithms with line impedances underestimated by 20%

the linear model is constructed based on underestimated line impedances. The voltages stay within the limit for the SGF, while the L-AC-OPF induces voltage magnitudes excursions outside of the admissible values. This shows that feedback-based algorithms are more robust to modeling uncertainties than traditional algorithms solved in an open-loop fashion.

Discussion on error in the measurements: One may say that feedback-based controllers are sensitive to measurement errors, which is true. However, traditional approaches to solving the AC-OPF also require measurements of load consumption, which are also subject to errors. The major difference is that for the proposed SGF algorithm, one can assess the maximum error on voltage measurements, and adapt the voltage thresholds to guarantee safe voltages throughout the network, e.g., if the voltage measurements are perturbed with a maximum error ε, one can tighten the voltage limits such that $[\mathbf{v}_{\min}, \mathbf{v}_{\max}]$ becomes $[\mathbf{v}_{\min} + \varepsilon, \mathbf{v}_{\max} - \varepsilon]$. For the L-AC-OPF, the error affects the load consumption, and one needs to propagate this error through the power system model to analyze the effect of those errors on voltages.

5 Conclusions

We have presented a feedback-based safe gradient flow controller for the optimal regulation of a VPP. The controller steers power injection of DERs to enforce voltage constraints at any time, and track power references at the substation. The controller does not necessitate load measurements at every node, and is robust against modeling errors due to the feedback addition. The controller has been tested on the IEEE37-node feeder, and compared with a linearized version of the AC-OPF. The results show superior performance of the feedback-based safe gradient flow controller compared to the linear AC-OPF, and constraint satisfaction even in the presence of modeling errors. Future work will consider a detailed robustness analysis of the controller against measurement errors, and additional assets such as batteries.

6 References

[1] Walling, R.A., Saint, R., Dugan, R.C., Burke, J., Kojovic, L.A.: 'Summary of distributed resources impact on power delivery systems', *IEEE Transactions on Power Delivery*, 2008, **23**, (3), pp. 1636–1644

[2] McDonald, J.: 'Solar power impacts power electronics in the smart grid', *Power Electronics*, 2013,

[3] Stanojev, O., Guo, Y., Aristidou, P., Hug, G.: 'Multiple ancillary services provision by distributed energy resources in active distribution networks', *arXiv preprint arXiv:220209403*, 2022,

[4] Dall'Anese, E., Guggilam, S.S., Simonetto, A., Chen, Y.C., Dhople, S.V.: 'Optimal regulation of virtual power plants', *IEEE Transactions on Power Systems*, 2017, **33**, (2), pp. 1868–1881

[5] Bernstein, A., Dall'Anese, E.: 'Real-time feedback-based optimization of distribution grids: A unified approach', *IEEE Transactions on Control of Network Systems*, 2019, **6**, (3), pp. 1197–1209

[6] Molzahn, D.K., Dörfler, F., Sandberg, H., Low, S.H., Chakrabarti, S., Baldick, R., et al.: 'A survey of distributed optimization and control algorithms for electric power systems', *IEEE Transactions on Smart Grid*, 2017, **8**, (6), pp. 2941–2962

[7] Singh, M.K., Kekatos, V., Giannakis, G.B.: 'Learning to solve the AC-OPF using sensitivity-informed deep neural networks', *IEEE Transactions on Power Systems*, 2021, **37**, (4), pp. 2833–2846

[8] Yuan, Z., Cavraro, G., Singh, M.K., Cortés, J.: 'Learning provably stable local volt/var controllers for efficient network operation', *IEEE Transactions on Power Systems*, 2023, **39**, (1), pp. 2066–2079

[9] Nellikkath, R., Chatzivasileiadis, S.: 'Physics-informed neural networks for AC optimal power flow', *Electric Power Systems Research*, 2022, **212**, pp. 108412

[10] Colot, A., Chen, Y., Cornélusse, B., Cortés, J., Dall'Anese, E.: 'Optimal power flow pursuit via feedback-based safe gradient flow', *arXiv preprint arXiv:231212267*, 2023,

[11] Allibhoy, A., Cortés, J.: 'Control-barrier-function-based design of gradient flows for constrained nonlinear programming', *IEEE Transactions on Automatic Control*, 2024, **69**, (6), pp. 3499–3514

[12] Bernstein, A., Wang, C., Dall'Anese, E., Le.Boudec, J.Y., Zhao, C.: 'Load flow in multiphase distribution networks: Existence, uniqueness, non-singularity and linear models', *IEEE Transactions on Power Systems*, 2018, **33**, (6), pp. 5832–5843

[13] Wang, C., Bernstein, A., Le.Boudec, J.Y., Paolone, M.: 'Existence and uniqueness of load-flow solutions in three-phase distribution networks', *IEEE Transactions on Power Systems*, 2017, **32**, (4), pp. 3319–3320

[14] Ames, A.D., Coogan, S., Egerstedt, M., Notomista, G., Sreenath, K., Tabuada, P.: 'Control barrier functions: Theory and applications', *Proc 18th European control conference (ECC)*, 2019, pp. 3420–3431